Tech Science Press

Synergistic Effect of Halloyosite Nanotube and Nanocellulose on Thermal and Mechanical Properties of Poly (Ethylmethacrylate-co-Acrylonitrile) Bionanocomposites

Karima Ben Hamou[1,2,*], Amal Kadimi[1], Remo Merijs Meri[3], Sergei Gaidukov[3], Hamid Kaddami[1], Mustapha Raihane[1], Mouhamed Lahcini[1] and Fouad Erchiqui[2]

[1]Laboratory of Organometallic and Macromolecular Chemistry - Composites Materials, Faculty of Sciences and Technology of Marrakech, Cadi Ayyad University, Guéliz, Av. A. El Khattabi, Marrakech, BP 618, Morocco
[2]Engineering School, University of Québec in Abitibi-Témiscamingue, 445 Boulevard de l'Université, Rouyn-Noranda, J9X 5E4, Québec, Canada
[3]Institute of Polymer Materials, Riga Technical University, Kaļķu iela 1, Centra rajons, Rīga, LV-1658, Latvia
*Corresponding Author: Karima Ben Hamou. Email: Karima.BenHamou@uqat.ca
Received: 31 July 2019; Accepted: 19 September 2019

Abstract: This work reports a comprehensive study on poly (Ethylmethacrylate-co-Acrylonitrile) Poly(EMA-AN) nanocomposites reinforced with a hybrid mixture of nanoreinforcements based on nanocrystals of cellulose (NCC) (1 or 5% wt) and halloysite nanotubes (HNTs) (1 or 5% wt). The morphology, thermal and mechanical properties of these nanocomposites were characterized. Homogeneous dispersion of the nanofillers has been shown by scanning electron microscopy. A significant increase of the rubbery modulus and glass transition temperature were obtained upon filler addition, due to the reduction of mobility of the matrix macromolecular chains. On the other hand, compared with the neat Poly(EMA-AN), the storage modulus of the nanocomposites increased by a factor 38 when adding 5 wt% NCC and by 17 for the same concentration of HNTs. mechanical properties of ternary nanocomposites were furthers increased resulting from a synergistic effect of these two nanofillers.

Keywords: Poly(Ethylmethacrylate-co-Acrylonitrile); nanocrystals cellulose; halloysite nanotubes; nanocomposites; hybrid; mechanical properties

1 Introduction

Polymer nanocomposites generally refer to organic/inorganic materials designed so that the matrix consists of a polymer to which an inorganic nanoscale particle is physically added or in which an inorganic species are grown under tightly controlled conditions to retain nanoscale dimensions and minimize aggregation.

Nowadays, functional and smart materials based on renewable bioresources and eco-friendly processes have attracted considerable attention. As the most abundant natural polymer in nature, cellulose is renewable, biodegradable, and biocompatible. It can be extensively derivatized to form strong and stable stiff-chain

homomolecular structure with fiber, film, and hydrogel-forming properties, which has the potential to be a stable and robust carrier, matrix, or scaffold component for the fabrication of functional materials [1-3].

Nanocrystals of cellulose (NCC) are promising candidates for nanocomposites production, owing to their large specific surface area, wide availability, biocompatibility and biodegradability, which may offer great opportunities to develop environmentally friendly structural composites. The most common method to extract NCC from natural fibers is sulfuric acid hydrolysis followed by centrifugation. The mechanism to isolate NCC is to destroy and remove non-crystalline regions, which are present between cellulose nanocrystals through chemical reactions. The sulfuric acid treatment introduces sulfate groups to the surface of NCC. The negative charges on the NCC surfaces lead to high stability of aqueous NCC suspension [4]. Favier et al. [5] were the first to explain the reinforcing effect of NCC in polymer matrixes. Formation of a mechanical percolation network was reported to be responsible for improvement of the mechanical properties. They investigated poly(styrene-co-butyl acrylate) latex/cellulose nanocrystal extracted from tunicin composite films prepared by solution casting. They showed that the shear modulus of the nanocomposites was improved over a wide temperature range above the glass transition temperature (T_g) of the matrix. The reason was explained by the development of percolating network of cellulose nanocrystals introduced by hydrogen bonding between neighboring cellulose nanocrystals. Recently, the combination of NCC with other nanostructured materials such as silver nanoparticles or nanosilica or clay mineral halloysite has been investigated as a promising strategy to further improve the performance of nanocomposites such as thermal, mechanical and barrier properties [6-11].

Layered halloysite occurs mainly in two different polymorphs, the hydrated form (with interlayer spacing of 10 Å) with the formula $Al_2Si_2O_5(OH)_4$ $2H_2O$ and the anhydrous form (with interlayer spacing of 7 Å) with the same chemical composition as kaolinite, $Al_2Si_2O_5(OH)_4$. The intercalated water is weakly held and can be readily and irreversibly removed [12,13]. Typically, HNTs are used in the manufacture of high quality ceramic white-ware [14] and are used as nanotemplates or nanoscale reaction vessels instead of carbon nanotubes (CNTs) or boron nitride nanotubes (BNNTs) [15,16]. Recently, several research teams have tried to utilize HNTs as nanofiller to enhance the functional properties of many polymers, such as natural rubber, nitrile rubber, polypropylene [17], ethylene-propylene-diene monomer copolymer (EPDM) [18], poly(ε-caprolactone) [19], pectin/polyethylene glycol [20] and polyvinyl alcohol (PVA) [10]. HNTs have drawn much attention also in the field of packaging due to their use as nanocarrier for controlled release of active compounds [21-23].

Growing concerns over environmental issues and the high demand for advanced polymeric materials with balanced properties have led to development of composite with hybrid natural reinforcement, of by combining different sizes (micro and nano) and types (organic and inorganic), as an alternative to synthetic fibers. The combination of nanofiller and natural fiber in the matrix demonstrate improved mechanical properties and a reduction in water absorption properties [24-28]. On the other hand the combination of nanofillers showed positive synergistic effects on mechanical and physical properties. For example, Bendahou et al. [11] investigated the synergistic effect of montmorillonite (MMT) and CNCs on the mechanical and barrier properties of natural rubber composites. However, the comparison of the effect of OMMT (Organo-modified MMT) and CNCs on the κ-carr films' physicochemical properties, which have SO_3 groups, was investigated by Zakuwan et al. [29]. In this study, the addition of hybrid reinforcement (CNC and OMMT) in κ-carr polymer improved composite-polymer interfacial interaction and the properties of the bionanocomposite.

A limited number of studies dealt with clay nanocomposites based on poly(ethyl methacrylate) and its copolymers with acrylonitrile or other monomers such styrene, methyl methacrylate, butadiene, or 2-hydroxy ethyl acrylate [30-40], but to the best of our knowledge, the preparation of nanocomposites based on poly (ethyl methacrylate-co-acrylonitrile) in presence of a hybrid nanofiller of fibrous clay mineral halloysite

and nanocrystals of cellulose (NCC), has not been reported. In the present work, thermal, physical, dielectric and dynamic properties of poly (ethyl methacrylate-co-acrylonitrile) nanocomposites filled by halloysite nanotubes and/or nanocrystals of cellulose (NCC) were studied. More importantly, the relationships among microstructure, dispersion and mechanical properties of poly (ethyl methacrylate-co-acrylonitrile) /NCC/HNTs nanocomposites were investigated. Halloysite nanotubes (HNTs), owing to their unique cylindrical shape and low density of hydroxyl functional groups, can be easily dispersed in polymer matrices even at high loading contents and do not require exfoliation like CNC and other nanoclays [41]. It's expected that the combination of these two nanofillers in the same material might improve the mechanical and physical properties and open perspectives of development of new active and materials of high performances.

2 Experimental Section

2.1 Materials

Acrylonitrile (AN) (bp. 77°C), and Ethylmethacrylate (EM) (bp. 100.5°C) are commercially available products (Fluka) and were distilled then stored below 25°C prior to use. Potassium Peroxodisulfate (KPS), Sodium dodecyl sulfate (SDS), Sodium Bicarbonate (NaHCO$_3$), Sulfuric acid (95%), N,N-Dimethylformamide (DMF), all the chemicals were obtained from Sigma–Aldrich. Halloysite nanotubes (HNTs) were kindly provided from Applied Mineral Incorporation and dried at 100°C under vacuum up to 24 h. Cellulose nanocrystals (NCC) extracted from the rachis of the palm of the date palm tree as described elsewhere [42-44].

2.2 Synthesis of Matrix

Into a glass reactor equipped with a mechanical stirring system and a reflux condenser, the surfactant (sodium dodecyl sulphate, SDS), buffer (sodium hydrogen carbonate, NaHCO$_3$), distilled water and the monomer(s) (acrylonitrile (AN) or/and ethyl methacrylate (EMA)) are introduced. This mixture is purged with nitrogen for 40 min and then placed in an oil bath, when the programmed temperature reaches 80°C, the initiator (potassium persulfate, KPS) previously dissolved in distilled water is introduced at one time and the polymerization starts. This mixture is left under mechanical stirring at 80°C, for 24 h to obtain latex. The free radical copolymerization product of ethyl methacrylate with acrylonitrile is prepared from an equimolar proportion of monomers (EMA/AN:50/50). The copolymer is prepared according to the scheme of Fig. 1.
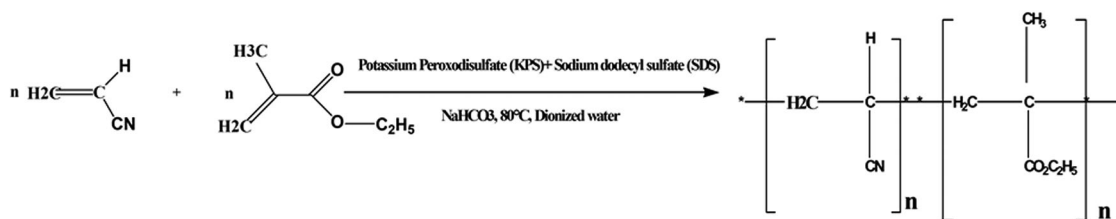

Figure 1: Synthetic scheme for poly(EMA-AN) (n = 50)

An aqueous solution of aluminum sulphate (10 wt%) is added to the latex in order to promote the separation of the polymer from the aqueous phase, the polymer obtained is then filtered and washed with distilled water to remove the residual surfactant, and then rinsed several times with methanol. The resulting product is then dried under vacuum at 60°C for 24 hours and characterized by FTIR, Proton Nuclear Magnetic Resonance spectroscopy (1H NMR), DSC and TGA analysis.

2.3 Preparation of Nanocomposite Films

Poly(EMA-AN) nanocomposite films reinforced with NCC and HNTs were prepared by solvent casting method in DMF. The aqueous suspension of cellulose nanocrystals was solvent-exchanged to acetone and then to DMF by several successive centrifugation and redispersion operations.

Poly(EMA-AN) was dissolved in DMF with vigorous stirring at room temperature for 24 h. The dissolved solution was poured into a Teflon Petri dish, and then allowed to dry for about one week at room temperature. For the preparation of the binary nanocomposite system, predetermined amounts of NCC (1&5 wt%) and HNTs (1&5 wt%) suspensions in DMF were mixed with the previously prepared Poly(EMA-AN) solution. The mixtures were stirred for one day by magnetic stirring and then sonicated by means of high power ultrasound disperser (Hielscher UIS250V ultrasound sonication equipment); degassed, then poured into a Teflon mold and placed at room temperature for two weeks to allow slow elimination of the solvent. Ternary composite films with 1 wt% or 5 wt% of NCC combined with 1 wt% and 5 wt% of HNTs were produced following the same procedure as described above and were subsequently characterized. All the systems were placed in a vacuum oven at 40°C for 2 weeks in order to remove all remaining DMF before testing. The ternary nanocomposites materials are referred as: Poly(EMA-AN)/NCC-x% /HNTs-y%, where x = 1 or 5 wt%, and y = 1 or 5 wt%; and the binary nanocomposite materials are referred as: Poly(EMA-AN)/NCC-x% or poly(EMA-AN)/HNTs-y%, where x = 1 or 5 wt%, and y = 1 or 5 wt%.

3 Characterization

3.1 Fourier Transform Infrared Spectrum (FTIR) Analysis

FTIR Spectra analyses were performed by Thermo Fischer Nicolet 6700 FTIR operated in Attenuated Total Reflection mode. 32 scans were used to obtain in the spectral in the wave range between 4000 and 400 cm^{-1} at a resolution of 4 cm^{-1}.

3.2 Differential Scanning Calorimetry (DSC)

DSC analysis was carried out using Mettler Toledo DSC1 equipped with Intracooler. A sample of 10 mg loaded in Aluminum pan was heated under N2 flux from room temperature to 100°C at a heating rate of 10°C/min followed by a cooling stage from 100 to −80°C at a cooling rate of 10°C/min. Finally, samples were repeatedly heated to 100°C at a heating rate of 10°C/min. The data were analyzed to determine the glass transition temperature Tg, from the second heating scan.

3.3 Thermogravimetric Analysis (TGA)

TGA was carried out with a Mettler Toledo TGA/DSC-1-SF apparatus at a heating rate of 10°C/min from room temperature up to 600°C, under nitrogen as the purge gas (60 mL/min).

3.4 Dynamic Mechanical Analysis (DMA)

DMA was performed using a dynamic mechanical analyzer (Mettler Toledo DMA/SDTA861). The data was recorded from 20 to 100°C at a heating rate of 3°C/min and a frequency of 1 Hz.

3.5 Scanning Electron Microscopy (SEM)

The morphology of the brittle fractured surface of the nanocomposite films was observed with a scanning electron microscope (FEI QUANTA 200F) at 5 kV and 10 A. the samples were fractured after being cooled in N liquid during 20 min to unsure a brittle fracture. The fractured surface was put on a conducting carbon tape stuck on the stub.

3.6 Nuclear Magnetic Resonance (NMR)

^{1}H NMR spectra were recorded under broad band decoupling on a Bruker AM 400 Mhz (pulse angle 70°, acquisition time 0.45 s, delay time 2 s), using deuterated chloroform as the solvents. The solvent signal was used as the internal standard.

4 Results and Discussion

By changing the loading of NCC and/or HNTs, a series of transparent Poly(EMA-AN) nanocomposites films were successfully prepared as shown in Fig. 2. It's worthy emphasizing that even with high content of nanofillers as 10 wt% (Fig. 2g) the nanocomposite is still transparent. This indicate a good dispersion of nanofillers in Poly (EMA-AN) matrix.

FTIR spectra of pure halloysite nanotubes (HNTs), cellulose nanocrystals (NCC), Poly(EMA-AN) copolymer and its nanocomposites materials are shown in Fig. 3. The spectrum of the NCC, Panel a of
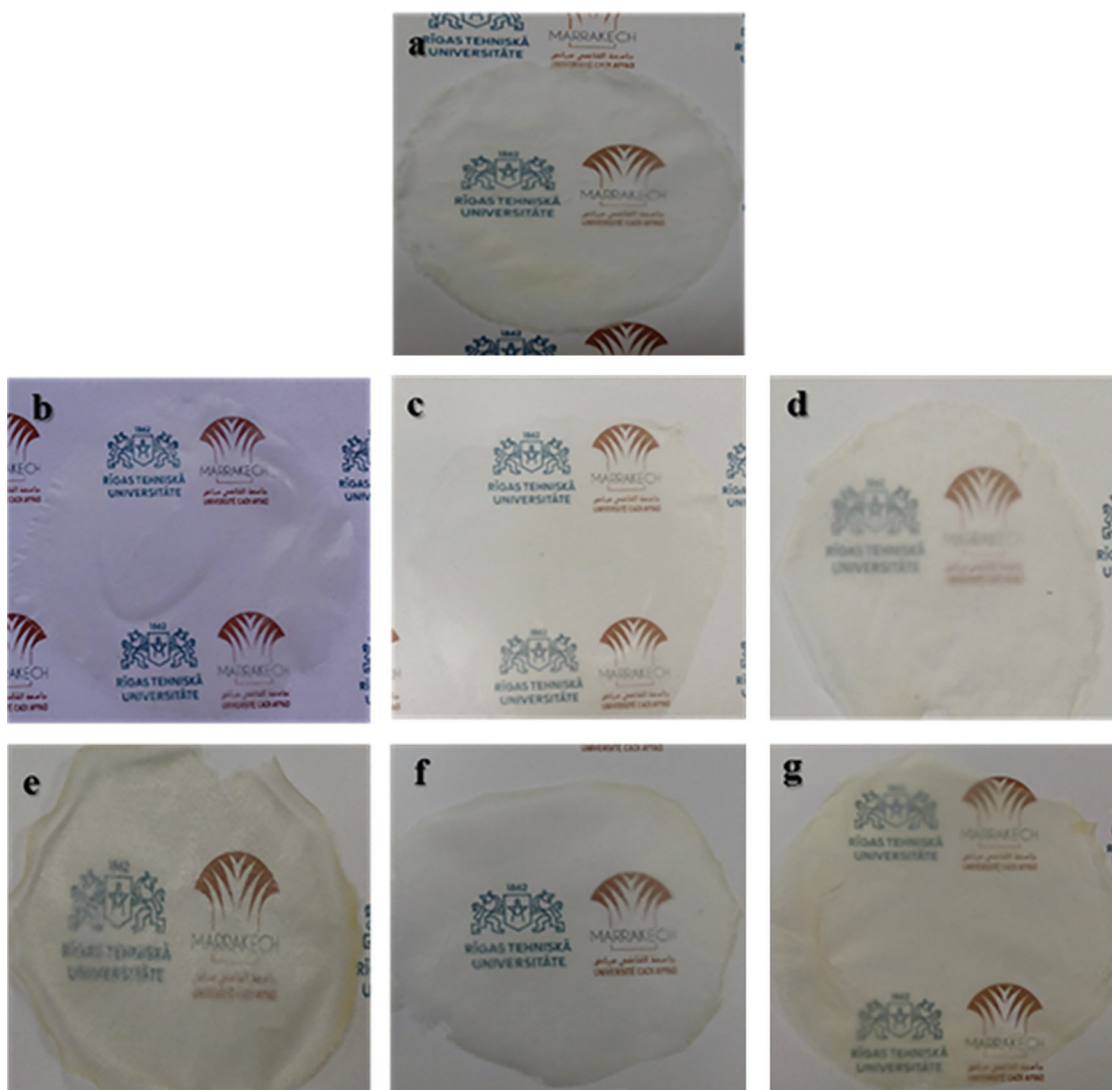

Figure 2: Digital photos of transparent nanocomposite samples with different wt.% of nanocrystals of cellulose and/or Halloysite Nanotubes. (a): neat matrix, (b): NCC-1%, (c): NCC-5%, (d): HNTs-1%, (e): HNTs-5%, (f): NCC-1%-HNTs-1% and (g) NCC-5%-HNTs-5%
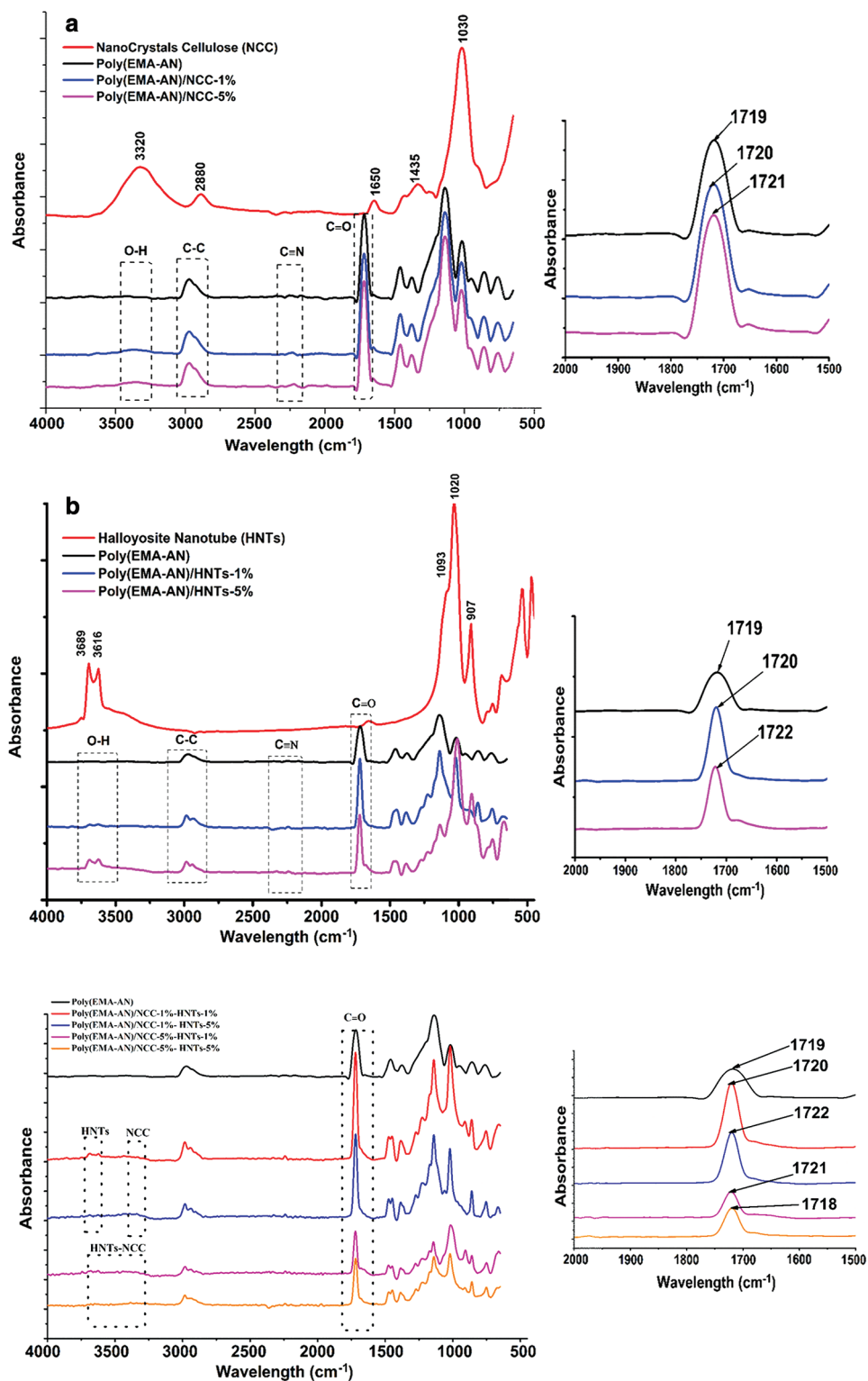
Figure 3: FTIR spectra of neat Poly(EMA-AN) and Poly(EMA-AN) nanocomposites

Fig. 3 shows the hydrogen- bonded stretching at 3320 cm^{-1}, the C–H stretching at 2880 cm^{-1}, the OH bending of the adsorbed water at 1650 cm^{-1}, the H–C–H and O–C–H in-plane bending vibrations at 1432 cm^{-1}. In addition, the bands at 1160, 1110, and 1060–1030 cm^{-1} correspond to C–O–C antisymmetric stretching, ring asymmetric stretching, and C–O stretching, respectively [45,46].

Figure 3b shows the characteristic peaks for HNTs. It was observed that the absorption band at 3616 cm^{-1} is the characteristic absorption of hydroxyl groups located on shared interfaces of layered structure consisting of silicon-oxygen tetrahedron and aluminium-oxygen octahedron, and the band at 3689 cm^{-1} is the characteristic absorption of external hydroxyl groups located on non-shared surfaces of the layered structure [47].The absorption bands nearby 1093 and 1020 cm^{-1} are assigned to stretching vibration of Si–O bonds. The characteristic absorption band at 907 cm^{-1} is due to flexural vibrations of Al–OH. The results confirm coexistence of hydroxyl groups and Si–O bonds at the surfaces of HNTs.

The spectrum of the neat Poly(EMA-AN), Figs. 3a and 3b, shows the formation of the copolymer due to the appearance of the bands at 2248 cm^{-1} (C≡N) and 1719 cm^{-1} (C=O) identifying the presence of acrylonitrile and ethyl methacrylate moieties of Poly(EMA-AN) respectively. The Poly(EMA-AN) copolymer was also characterized by ^{1}H NMR. Tab. 1 displays the 1H NMR chemical shifts for our copolymer. Original ^{1}H NMR spectrum of Poly(EMA-AN) is shown in Supplementary Fig. S1.

Table 1: ^{1}H NMR chemical shifts for Poly (EMA-AN) copolymer

Comonomer unit	Species	^{1}H δ (ppm)
AN	**CH**CN	1.6-2.2
EMA	**CH₂**	
	CH₂(main chain)	1.3-1.63
	CH₃	
	CH₂**CH₃**	
	CH₂CH₃	4.056-4.14

The chemical shift assignments of Poly(EMA-AN) copolymer recorded in chloroform-d6 were deduced from the comparison with those of polymers based on AN [48, 49]. Tab. 1 shows the chemical shifts of different protons in the copolymer. It also exhibits the absence of the vinyl peaks bound to the monomer unit CH$_2$ (5.5-6.15) of the EMA as well as that CH$_2$ (5.8-6) of the AN and thus confirms the success of such a copolymerization

The presence of cellulose nanocrystals and halloysite nanotubes in Poly(EMA-AN) matrix (Figs. 3a and 3b) leads to the appearance of the peak of –OH stretching (centered at 3616-3689 cm^{-1} for Poly(EMA-AN)/ HNTs and at 3375 cm^{-1} for Poly(EMA-AN)/NCC). Compared to the Poly(EMA-AN) binary films, the FTIR spectra of ternary system Poly(EMA-AN)/NCC-HNTs (Fig. 3c) shows the shifted bands of carbonyl groupments C=O to higher wave numbers with the different hybrids, indicating the presence of interactions that occurred between the Poly(EMA-AN) and the NCC/HNTs as illustrated in the scale expanded FTIR spectra in Fig. 3c. Smaller shifts of the two peaks of HNTs and NCC, ascribed to the bending of OH groups, shift toward higher wavenumbers. This shift was explained by Aloui et al. [10] to the establishment of specific interactions between NCC and HNT, i.e., H-bonding interactions between

the hydroxyls of NCC with the more accessible ones of HNT particles, which avoid aggregations and allow a good dispersion within the polymeric matrix. This could also indicate a mutual emulsification of the two particles preventing their own aggregations [50,51].

The SEM images of binary and ternary nanocomposites fracture surfaces were observed in order to evaluate the samples morphology and to analyze the dispersion of cellulose nanocrystals and halloysites nanotubes inside the polymer matrix. SEM images in Figs. 4a–4e reveal micro-sized white domains on the fracture surfaces of the Poly(EMA-AN)/HNTs nanocomposites. These fine white particles are HNTs clusters and are evenly distributed in the matrix. The absence of parting lines, voids and cavities in the micrographs suggest that there is a very good wetting and adhesion bonding among Poly(EMA-AN)/ and HNTs. Whereas NCC aggregates during the evaporation of the solvent forming wrinkle features, ascribed to the assembling of NCC. According to the Figs. 4f–4k, there was no evidence of micrometer scale agglomerates of NCC. Good dispersion and percolating network structure formation of NCC were
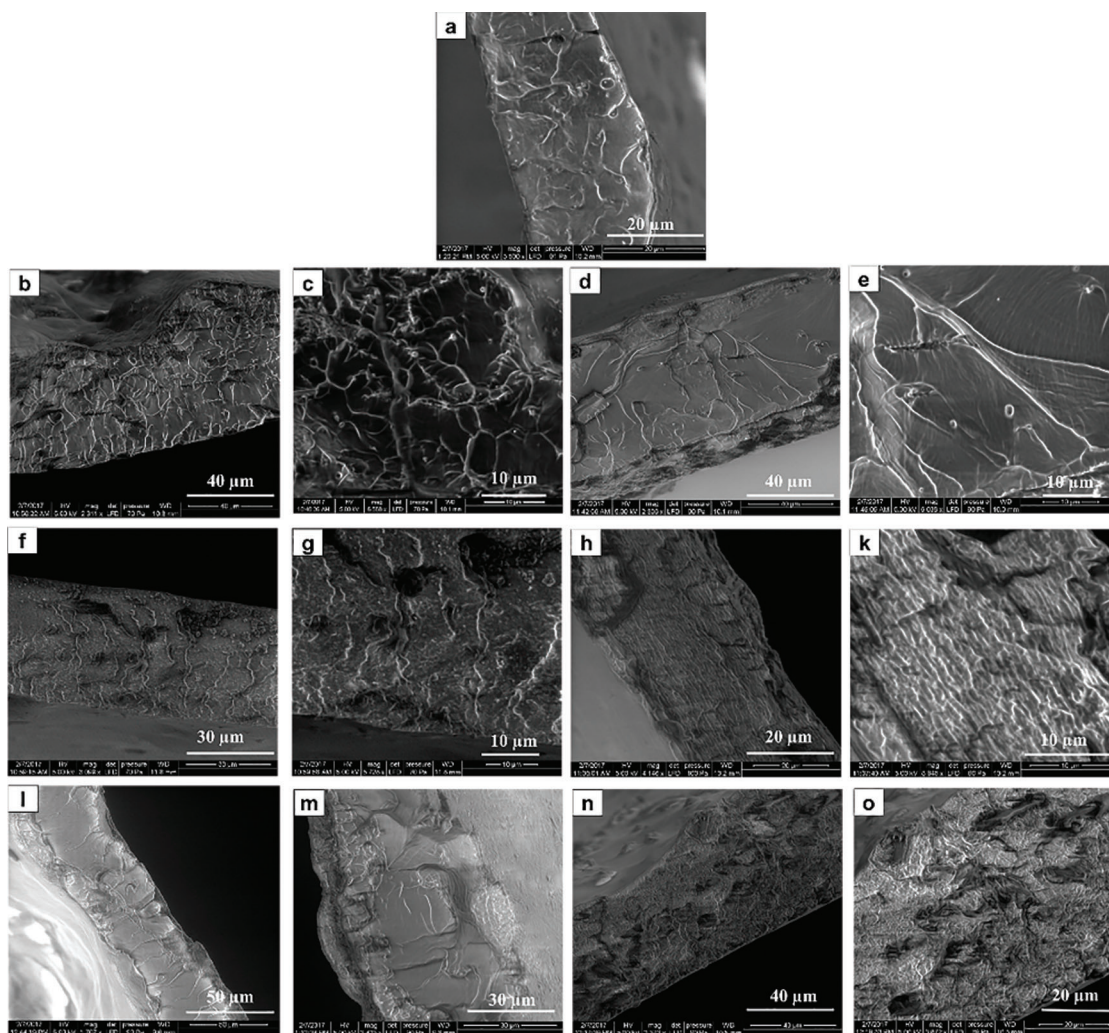

Figure 4: Scanning electron microscopy images of (a) neat Poly(EMA-AN), (b) and (c) Poly(EMA-AN)/ HNTs-1%, (d) and (e) Poly(EMA-AN)/HNTs-5%, (f) and (g) Poly(EMA-AN)/NCC-1%, (h) and (k) Poly (EMA-AN)/NCC-5%, (l) and (m) Poly(EMA-AN)/NCC-1%-HNTs-1%, (n) and (o) Poly(EMA-AN)/ NCC-5%,-HNTs-5% nanocomposites

significant to the transparency of the investigated polymer/NCC nanocomposites. SEM micrographs of ternary Poly(EMA-AN) nanocomposites show that the presence of NCC and HNTs allows a better dispersion in the neat matrix without the formation of surface wrinkles in comparison to the binary nanocomposite (Figs. 4l–4o). This can be attributed to specific interactions between NCC and HNTs, i.e., H-bonding interactions between the hydroxyls of NCC with the more accessible hydroxyls of HNT particles, which avoid aggregations and allow a good dispersion within the polymeric matrix, which testifies the synergistic action of HNTs coupled with NCC filler in the improvement of reciprocal dispersion within polymeric nanocomposites.

To further investigate the interactions between the nanofiller and the host copolymer, DSC analyses were performed for unfilled and filled samples. Tab. 2 gathers the thermal proprieties temperature of neat Poly(EMA-AN) and its corresponding nanocomposites. Original DSC thermograms of Poly(EMA-AN) and Poly(EMA-AN) nanocomposites are shown in Supplementary Fig. S2.

Table 2: DSC. TGA and DMA data for Poly (EMA-AN) nanocomposites and Poly(EMA-AN) reference. Onset glass transition temperature ($T_{g\ onset}$), degradation temperature (T_{d1}), char yield at 600°C, storage modulus at 80°C ($E'_{80°C}$), reinforcement factor R_f, and the synergy ratio. The values of the modulus were normalized at low temperature.

	DSC Data	DMA Data			TGA Data	
	$T_{g\ onset}$ (°C)	E' (80°C) (MPa)	R_f	The Synergy effect	T_{d1} (°C)	Char yield at 600°C (wt%)
Neat Poly(EMA-AN)	58	6.49	1	–	280	1.40
Poly(EMA-AN)/NCC-1%	63	62.75	10	–	275-	2.72
Poly(EMA-AN)/NCC-5%	64	247.80	38	–	245	5.43
Poly(EMA-AN)/HNTs-1%	61	52.10	8	–	286	2.84
Poly(EMA-AN)/HNTs-5%	63	108.39	17	–	281	5.92
Poly(EMA-AN)/NCC-1%-HNTs-1%	62	63.88	10	0.55	306	3.54
Poly(EMA-AN)/NCC-1%-HNTs-5%	65	364.44	56	2.13	268	7.97
Poly(EMA-AN)/NCC-5%/HNTs-1%	64	442.14	68	1.47	285	6.82
Poly(EMA-AN)/NCC-5%/HNTs-5%	64	193.76	29	0.52	257	12.25

The DSC thermograms of the copolymer exhibit one glass transition temperature (T_g) suggesting a random structure of EMA/AN copolymer. The $T_g(s)$ of random EMA/AN copolymers were also studied by Penzel et al. [52,53] showing good agreement with the T_g of the copolymers investigated in this research.

Globally, it was observed that the $T_{g\ onset}$ values of binary and ternary nanocomposites are significantly higher than that of the neat copolymer. This is due to the strong interactions between the copolymer and the nanofiller via hydrogen bonding which restrict the mobility of the segments of the copolymer [54,55]. A similar result of the increasing of glass transition of polymer after the introduction of rigid nanoparticles was also reported for the nanocomposites of poly(propylenecarbonate) /cellulose nanocrystals [56], and poly(3-hydroxybutyrate-co-3 hydroxyvalerate)/cellulose nanowhisker [57].

The thermal stability and degradation profiles of the nanocomposite films were assessed using thermogravimetric analysis. Fig. 5 shows the TGA curves of binary and ternary nanocomposites with different contents of NCC and HNTs. The data reveals that all nanocomposites demonstrated single-stage thermal degradation. The pure copolymer displayed at 280°C; however, binary nanocomposites with 1 and 5% wt of NCC started degradation at 275 and 245°C, respectively. This shows a significant reduction of thermal stability by inclusion of NCC as widely confirmed in literature [58,59]. In the case of poly(EMA-AN)/HNTs binary nanocomposites, the thermal degradation occurs slightly at higher temperature (i.e., 285°C for Poly(EMA-AN)/ HNTs-5% vs. 280°C for neat poly(EMA-AN).
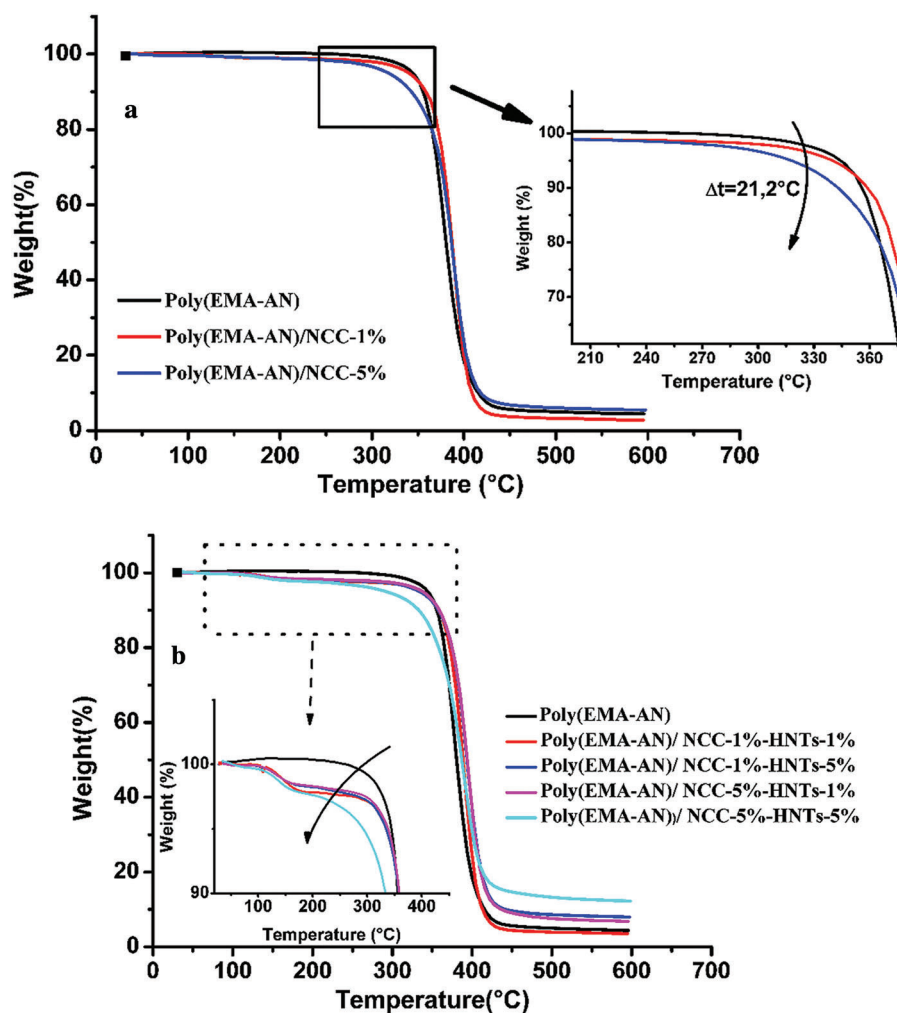

Figure 5: TGA curves of Poly(EMA-AN) and Poly(EMA-AN) nanocomposites. (a): Poly(EMA-AN)/NCC, (b): Poly(EMA-AN)/NCC-HNTs

Moreover, two-step weight loss process was observed for the combination of HNTs with NCC in the copolymer matrix. The low temperature process starting from 45°C to 100°C is most probably ascribed to the evaporation of residual water and the second weight loss process related to the decomposition of the Poly(EMA-AN) copolymer with an observed decrease of T_{d1} with the presence of HNTs nanoparticles. Samples with NCC-1%-HNTs-1% and NCC-5%-HNTs-1% started degradation at 306 and 285°C,

respectively, thus demonstrating slightly higher thermal stability. The decomposition of samples continued until temperatures rose above 500°C at which point a constant mass was achieved. The residue content at 600°C was also determined and is summarized in Tab. 2. Higher residual masses were observed in the case of ternary systems, most likely due to the different degradation mechanism occurring in the case of ternary systems.

The dynamical mechanical properties of the Poly(EMA-AN) and its nanocomposites studied by DMA measurements are presented in Fig. 6 and Tab. 2. DMA is a very suitable tool to investigate the viscoelastic properties of materials in a wide range of temperatures. Modulus values have been normalized at low temperature to allow a better comparison.
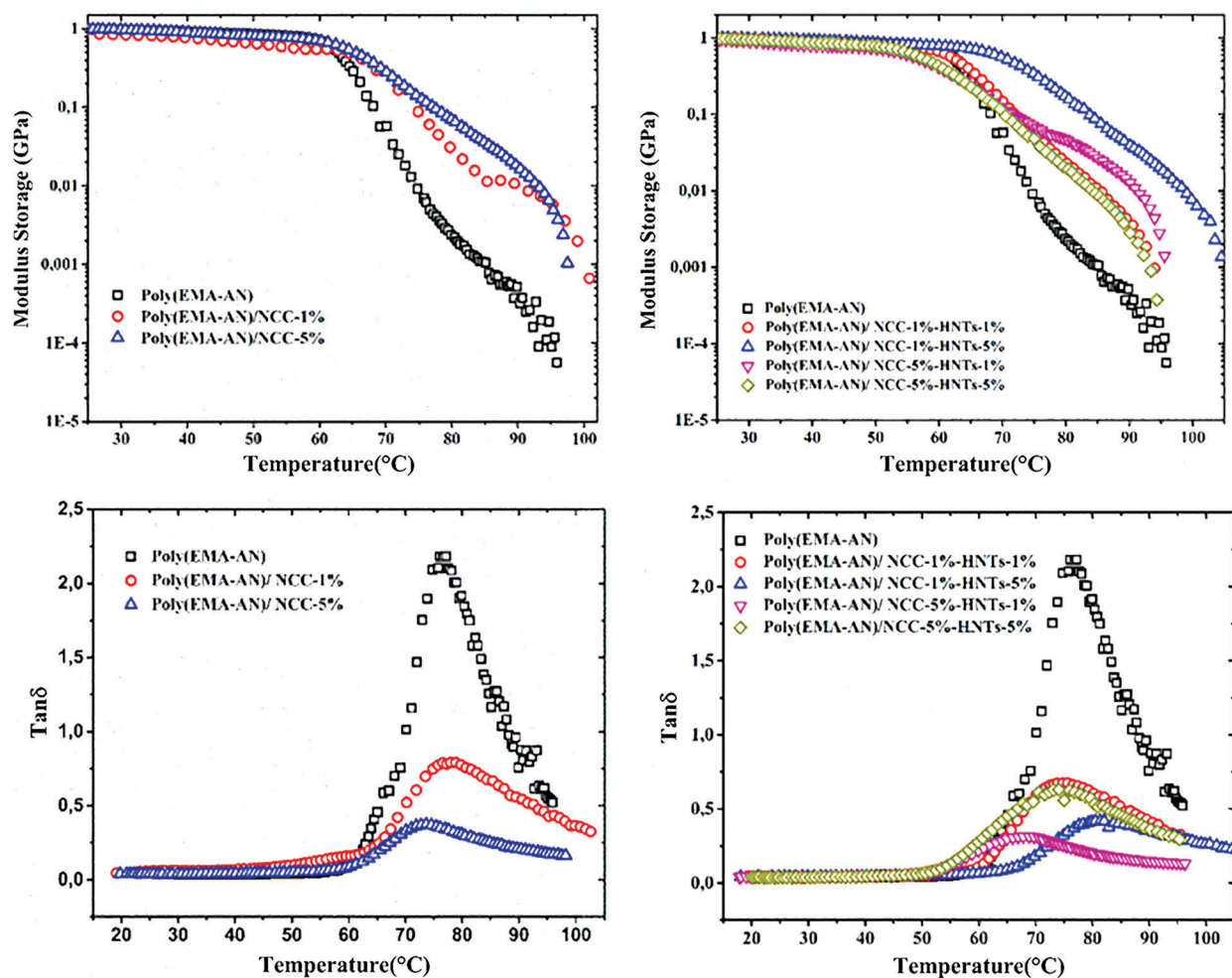

Figure 6: Storage modulus (E′) curves as a function of temperature of Poly(EMA-AN) and Poly(EMA-AN) nanocomposites with different NCC and/or HNTs contents

First, it should be highlighted that the presence of the nanofillers had a remarkable effect on the viscoelastic properties of the resulting nanocomposites, regardless the filler type (NCC or HNTs) and its content. This was demonstrated by an increase of the rubbery storage modulus and a decrease in the magnitude of the tanδ peak. Such improvement in dynamic mechanical properties of the produced Poly(EMA-AN) nanocomposites could be attributed to the good interfacial adhesion between the

incorporated fillers and the copolymer matrix, along with their homogeneous dispersion in the polymeric matrix which may result in an efficient load transfer between polymer chains and the nanofillers [60], outlining the ability of these two nanofillers, either alone or in combination, to improve the plastic response of the reinforced material.

We defined a reinforcing factor, R_f, as the ratio between the storage modulus for each nanocomposite divided by the storage modulus of neat Poly(EMA-AN) at the same temperature, i.e., the R_f value corresponds to the number of times the storage modulus was increased by the presence of the fibrils [61]. The R_f values estimated at 80°C are collected in Tab. 2 and presented in Fig. 7.
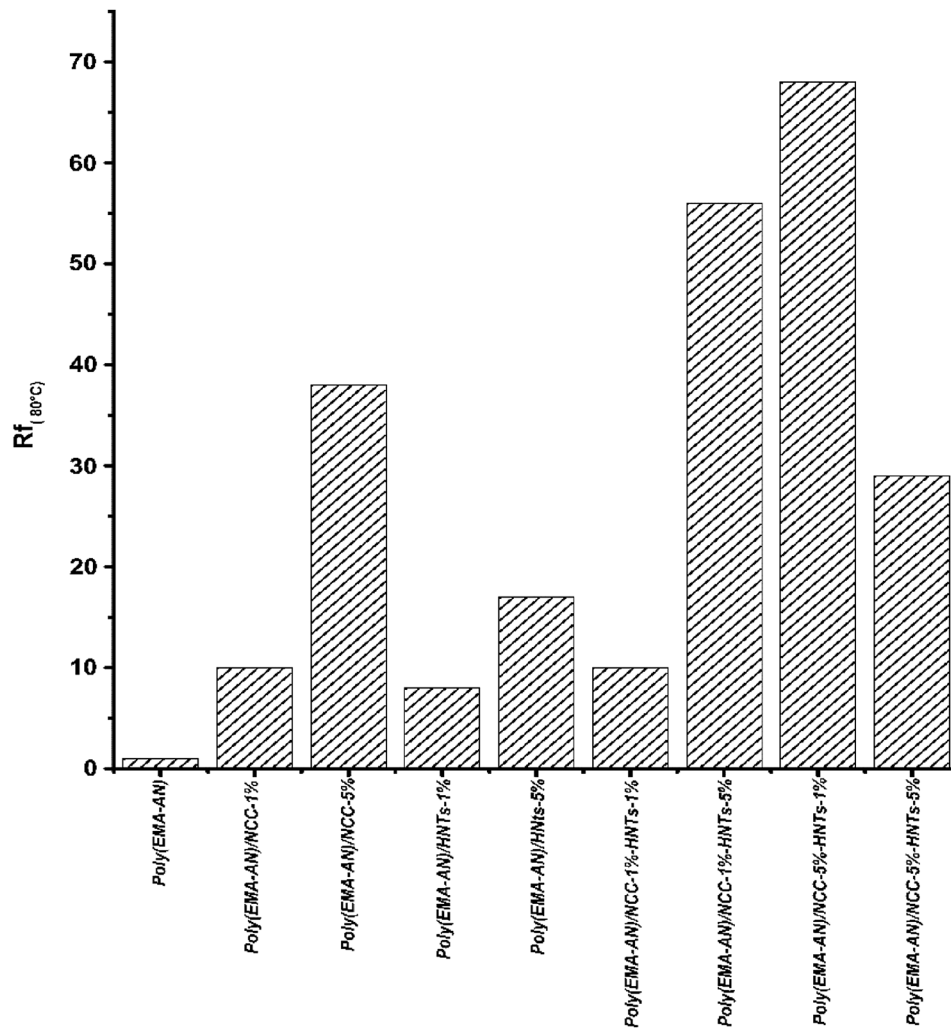

Figure 7: Reinforcing factor (R_f) at 80°C of Poly(EMA-AN) and Poly(EMA-AN) nanocomposites with different NCC and/or HNTs contents

For each type of fibril, the R_f values dramatically increased with increasing fibril contents. For example, the storage modulus of the Poly(EMA-AN) matrix increased by a factor of 38 when adding 5 wt% NCC vs. 17 for the same concentration of HNTs. This effect is attributed to the well-known reinforcing effect induced

by the presence of the nanofibril network [43,44,62-65]. For ternary nanocomposites, the addition of NCC into Poly(EMA-AN) matrix and Poly(EMA-AN)/HNTs nanocomposites significantly increases the mechanical properties compared to neat copolymer and its nanocomposites. This is due to the unique properties of cellulose fibers in enhancement of polymer mechanical properties [66,67]. The addition of NCC to the Poly(EMA-AN)/HNTs nanocomposites is found to have a positive effect on storage modulus when compared with unfilled Poly(EMA-AN)/HNTs nanocomposites.

This improvement in viscoelastic properties can be related to the enhanced NCC- matrix interface due to the presence of HNT tubes. More interestingly, the presence of the fibrils also led to the gradual decreasing of the tan δ peak with increasing fibrils contents. These effects are associated with the segmental motions of the poly(EMA-AN) chains being increasingly restricted by the presence of the nanofillers network and their strong interaction with the highly hydrophilic poly(EMA-AN).

When considering all nanocomposites at any given fibril content, the ternary system clearly showed the highest R_f values at 80°C compared to poly(EMA-AN) and binary nanocomposites.

In fact, a synergistic effect between the fibril types was found for NCC-1%-HNTs-5% and NCC-5%-HNTs-1% fibril loadings at 80°C. This is shown by a synergy ratio, defined as the Rf provided by the NCC and HNTs divided by the sum of the individual R_{fs} due to the NCC and the HNTs, greater than 1 for these compositions (Tab. 2). As expected, this synergistic effect was more significant for hybrid nanocomposites prepared with NCC-1%-HNTs-5% and NCC-5%-HNTs-with ratios around 2.13 and 1.47, suggesting that the 6% wt of NCC-HNTs nanofillers form the most effective percolating network within the poly(EMA-AN) matrix. As the fibril content increased, the synergistic effect was progressively reduced and it vanished for nanocomposites with 10% wt (NCC-5%-HNTs-5%) (ratio < 1).

5 Conclusions

Poly(EMA-AN)/NCC and/or HNTs nanocomposites were prepared by solvent exchange and solution casting techniques. The obtained Poly(EMA-AN)/NCC and/or HNTs films containing of 1 and 5 wt% NCC and/or HNTs were highly transparent.

The nature and the amount of NCC and HNTs nanofillers markedly influenced the properties of the Poly(EMA-AN) nanocomposites. The morphological studies indicated that NCC and/or HNTs were uniformly dispersed in the copolymer matrix. Mechanical tests showed that the storage modulus of the nanocomposites increased dramatically with increasing NCC and/or HNTs content. Compared with the neat Poly(EMA-AN), the storage modulus of the Poly(EMA-AN) matrix increased by a factor 38 when adding 5 wt% NCC *vs*. 17 for the same concentration of HNTs. Addition of NCC into Poly(EMA-AN) matrix and Poly(EMA-AN)/HNTs nanocomposites significantly increased mechanical properties of ternary nanocomposites.

The thermal analysis indicated that introduction of NCC and/or HNTs into Poly(EMA-AN) led to an decrease in the thermal stability. However, the thermal stability of Poly(EMA-AN)/NCC-HNTs nanocomposites is slightly higher than that of binary systems owing to the to the contribution of NCC-HNTs as an effective nucleating agent.

Conflicts of Interest: The authors declare that they have no conflicts of interest to report regarding the present study.

References

1. Shi, Z., Phillips, G. O., Yang, G. (2013). Nanocellulose electroconductive composites. *Nanoscale, 5(8),* 3194–3201. DOI 10.1039/c3nr00408b.

2. Kim, J., Yun, S., Ounaies, Z. (2006). Discovery of cellulose as a smart material. *Macromolecules, 39(12),* 4202–4206. DOI 10.1021/ma060261e.

3. Qi, H., Liu, J., Gao, S., Mäder, E. (2013). Multifunctional films composed of carbon nanotubes and cellulose regenerated from alkaline–urea solution. *Journal of Materials Chemistry A, 1(6),* 2161–2168. DOI 10.1039/C2TA00882C.

4. Bondeson, D., Mathew, A., Oksman, K. (2006). Optimization of the isolation of nanocrystals from microcrystalline cellulose by acid hydrolysis. *Cellulose, 13(2),* 171–180. DOI 10.1007/s10570-006-9061-4.

5. Favier, V., Chanzy, H., Cavaille, J. Y. (1995). Polymer nanocomposites reinforced by cellulose whiskers. *Macromolecules, 28(18),* 6365–6367. DOI 10.1021/ma00122a053.

6. Xu, X., Yang, Y. Q., Xing, Y. Y., Yang, J. F., Wang, S. F. (2013). Properties of novel polyvinyl alcohol/cellulose nanocrystals/silver nanoparticles blend membranes. *Carbohydrate Polymers, 98(2),* 1573–1577. DOI 10.1016/j.carbpol.2013.07.065.

7. Fortunati, E., Peltzer, M., Armentano, I., Jiménez, A., Kenny, J. M. (2013). Combined effects of cellulose nanocrystals and silver nanoparticles on the barrier and migration properties of PLA nano-biocomposites. *Journal of Food Engineering, 118(1),* 117–124. DOI 10.1016/j.jfoodeng.2013.03.025.

8. Fortunati, E., Rinaldi, S., Peltzer, M., Bloise, N., Visai, L. et al. (2014). Nano-biocomposite films with modified cellulose nanocrystals and synthesized silver nanoparticles. *Carbohydrate Polymer, 101,* 1122–1133. DOI 10.1016/j.carbpol.2013.10.055.

9. Ching, Y. C., Rahman, A., Ching, K. Y., Sukiman, N. L., Chuah, C. H. (2015). Preparation and characterization of polyvinyl alcohol-based composite reinforced with nanocellulose and nanosilica. *BioResources, 10(2),* 3364–3377. DOI 10.15376/biores.10.2.3364-3377.

10. Aloui, H., Khwaldia, K., Hamdi, M., Fortunati, E., Kenny, J. M. et al. (2016). Synergistic effect of halloysite and cellulose nanocrystals on functional properties of PVA based nanocomposites. *ACS Sustainable Chemistry & Engineering, 4(3),* 794–800. DOI 10.1021/acssuschemeng.5b00806.

11. Bendahou, A., Kaddami, H., Espuche, E., Gouanve, F., Dufresne, A. (2011). Synergism effect of montmorillonite and cellulose whiskers on the mechanical and barrier properties of natural rubber composites. *Macromolecular Materials and Engineering, 296(8),* 760–769. DOI 10.1002/mame.201000444.

12. Guimarães, L., Enyashin, A. N., Seifert, G., Duarte, H. A. (2010). Structural, electronic, and mechanical properties of single-walled halloysite nanotube models. *Journal of Physical Chemistry C, 114(26),* 11358–11363. DOI 10.1021/jp100902e.

13. Joussein, E., Petit, S., Churchman, J., Theng, B., Righi, D. et al. (2005). Halloysite clay minerals – a review. *Clay Minerals, 40(4),* 383–426. DOI 10.1180/0009855054040180.

14. Noro, H. (1986). Hexagonal platy halloysite in an altered tuff bed, Komaki City, Aichi Prefecture, Central Japan. *Clay Minerals, 21(3),* 401–415. DOI 10.1180/claymin.1986.021.3.11.

15. Sarah, A. (2003). Halloysite: a low-cost alternative nanotube. *Australian Journal of Chemistry, 56(7),* 723–723. DOI 10.1071/CH03099.

16. Shchukin, D. G., Sukhorukov, G. B., Price, R. R., Lvov, Y. M. (2005). Halloysite nanotubes as biomimetic nanoreactors. *Small, 1(5),* 510–513. DOI 10.1002/smll.200400120.

17. Du, M., Guo, B., Jia, D. (2006). Thermal stability and flame-retardant effects of halloysite nanotubes on poly (propylene). *European Polymer Journal, 42(6),* 1362–1369. DOI 10.1016/j.eurpolymj.2005.12.006.

18. Ismail, H., Pasbakhsh, P., Fauzi, M. N. A., Abu Bakar, A. (2008). Morphological, thermal and tensile properties of halloysite nanotubes filled ethylene propylene diene monomer (EPDM) nanocomposites. *Polymer Testing, 27(7),* 841–850. DOI 10.1016/j.polymertesting.2008.06.007.

19. Lahcini, M., Elhakioui, S., Szopinski, D., Neuer, B., El Kadib, A. et al. (2016). Harnessing synergies in tin-clay catalyst for the preparation of poly(ε-caprolactone)/halloysite nanocomposites. *European Polymer Journal, 81,* 1–11. DOI 10.1016/j.eurpolymj.2016.05.014.

20. Cavallaro, G., Lazzara, G., Milioto, S. (2013). Sustainable nanocomposites based on halloysite nanotubes and pectin/polyethylene glycol blend. *Polymer Degradation and Stability, 98(12),* 2529–2536. DOI 10.1016/j.polymdegradstab.2013.09.012.

21. Lee, M. H., Park, H. J. (2015). Preparation of halloysite nanotubes coated with Eudragit for a controlled release of thyme essential oil. *Journal of Applied Polymer Science, 132,* 42771– 42778.

22. Gorrasi, G. (2015). Dispersion of halloysite loaded with natural antimicrobials into pectins: characterization and controlled release analysis. *Carbohydrate Polymers, 127,* 47–53. DOI 10.1016/j.carbpol.2015.03.050.

23. Tornuk, F., Hancer, M., Sagdic, O., Yetim, H. (2015). LLDPE based food packaging incorporated with nanoclays grafted with bioactive compounds to extend shelf life of some meat products. *LWT - Food Science and Technology, 64(2),* 540–546. DOI 10.1016/j.lwt.2015.06.030.

24. Lee, K. Y., Bharadia, P., Blaker, J. J., Bismarck, A. (2012). Short sisal fibre reinforced bacterial cellulose polylactide nanocomposites using hairy sisal fibres as reinforcement. *Composites Part A: Applied Science and Manufacturing, 43(11),* 2065–2074. DOI 10.1016/j.compositesa.2012.06.013.

25. Hajlane, A., Kaddami, H., Joffe, R., Wallström, L. (2013). Design and characterization of cellulose fibers with hierarchical structure for polymer reinforcement. *Cellulose, 20(6),* 2765–2778. DOI 10.1007/s10570-013-0044-y.

26. Hajlane, A., Joffe, R., Kaddami, H. (2018). Nanocrystal deposition onto regenerated cellulose fibres: effect on moisture absorption and fibre-matrix adhesion. *Cellulose, 25(3),* 1783–1793. DOI 10.1007/s10570-018-1680-z.

27. Cavallaro, G., Lazzara, G., Milioto, S., Parisi, F., Evtugyn, V. et al. (2018). Nanohydrogel formation within the halloysite lumen for triggered and sustained release. *ACS Applied Materials & Interfaces, 10(9),* 8265–8273. DOI 10.1021/acsami.7b19361.

28. Bertolino, V., Cavallaro, G., Lazzara, G., Milioto, S., Parisi, F. (2017). Biopolymer-targeted adsorption onto halloysite nanotubes in aqueous media. *Langmuir, 33(13),* 3317–3323. DOI 10.1021/acs.langmuir.7b00600.

29. Zakuwan, S., Ahmad, Z. I. (2018). Synergistic effect of hybridized cellulose nanocrystals and organically modified montmorillonite on κ-carrageenan bionanocomposites. *Nanomaterials, 8(11),* 874. DOI 10.3390/nano8110874.

30. Lim, S. K., Kim, J. W., Chin, I., Kwon, Y. K., Choi, H. J. (2002). Preparation and interaction characteristics of organically modified montmorillonite nanocomposite with miscible polymer blend of poly(ethylene oxide) and poly(methyl methacrylate). *Chemistry of Materials, 14(5),* 1989–1994. DOI 10.1021/cm010498j.

31. Li, Y., Ishida, H. (2003). Solution intercalation of polystyrene and the comparison with poly(ethyl methacrylate). *Polymer, 44(21),* 6571–6577. DOI 10.1016/S0032-3861(03)00683-9.

32. Wilder, E. A., Braunfeld, M. B., Jinnai, H., Hall, C. K., Agard, D. A. et al. (2003). Nanofibrillar networks in poly(ethyl methacrylate) and its silica nanocomposites. *The Journal of Physical Chemistry B, 107(42),* 11633–11642. DOI 10.1021/jp035113u.

33. Kim, M. S., Jun, J. K., Jeong, H. M. (2008). Shape memory and physical properties of poly(ethyl methacrylate)/Na-MMT nanocomposites prepared by macroazoinitiator intercalated in Na-MMT. *Composites Science and Technology, 68(7-8),* 1919–1926. DOI 10.1016/j.compscitech.2007.12.015.

34. Barkoula, N. M., Alcock, B., Cabrera, N. O., Peijs, T. (2008). Fatigue properties of highly oriented polypropylene tapes and all-polypropylene composites. *Polymers and Polymer Composites, 16(2),* 101–113. DOI 10.1177/096739110801600203.

35. Ouaad, K., Djadoun, S., Vincent, L., Sbirrazzuoli, N. (2013). Elaboration and thermal behavior of nanocomposites based on poly (ethyl methacrylate) and an Algerian bentonite prepared via in situ polymerization initiated by Ni (II)α-benzoinoxime complex. *Thermochimica Acta, 555,* 30–36. DOI 10.1016/j.tca.2012.12.017.

36. Kadi, S. (2015). Thermal behavior of poly (ethyl methacrylate-co-acrylonitrile) nanocomposites prepared in the presence of an Algerian bentonite via solution intercalation and in situ polymerization. *Journal of Thermal Analysis and Calorimetry, 119(2),* 1113–1122. DOI 10.1007/s10973-014-4263-8.

37. Vallés-Lluch, A., Rodríguez-Hernández, J. C., Ferrer, G. G., Pradas, M. M. (2010). Synthesis and characterization of poly(EMA-co-HEA)/SiO$_2$ nanohybrids. *European Polymer Journal, 46(7),* 1446–1455. DOI 10.1016/j.eurpolymj.2010.04.010.

38. Voulgaris, D., Petridis, D. (2002). Emulsifying effect of dimethyldioctadecylammonium-hectorite in polystyrene/poly(ethyl methacrylate) blends. *Polymer (Guildf), 43(8),* 2213–2218. DOI 10.1016/S0032-3861(02)00039-3.

39. Kiran Kumar, A. B. V., Daniel Thangadurai, T., Lee, Y. I. (2013). Poly [2-(cinnamoyloxy)ethyl methacrylate-co-octamethacryl-POSS] nanocomposites: synthesis and properties. *Reactive and Functional Polymers, 73(9),* 1175–1179. DOI 10.1016/j.reactfunctpolym.2013.05.010.

40. Vallés-Lluch, A., Gallego Ferrer, G., Pradas, M. M. (2010). Effect of the silica content on the physico-chemical and relaxation properties of hybrid polymer/silica nanocomposites of P(EMA-co-HEA). *European Polymer Journal, 46(5),* 910–917. DOI 10.1016/j.eurpolymj.2010.02.004.

41. Prashantha, K., Lecouvet, B., Sclavons, M., Lacrampe, M. F., Krawczak, P. (2013). Poly(lactic acid)/halloysite nanotubes nanocomposites: structure, thermal, and mechanical properties as a function of halloysite treatment. *Journal of Applied Polymer Science, 123,* 1895–1903.

42. Marchessault, R. H., Morehead, F. F., Walter, N. M. (1959). Liquid crystal systems from fibrillar polysaccharides. *Nature, 184(4686),* 632–633. DOI 10.1038/184632a0.

43. Bendahou, A., Kaddami, H., Dufresne, A. (2010). Investigation on the effect of cellulosic nanoparticles' morphology on the properties of natural rubber based nanocomposites. *European Polymer Journal, 46(4),* 609–620. DOI 10.1016/j.eurpolymj.2009.12.025.

44. Benhamou, K., Kaddami, H., Magnin, A., Dufresne, A., Ahmad, A. (2015). Bio-based polyurethane reinforced with cellulose nanofibers: a comprehensive investigation on the effect of interface. *Carbohydrate Polymers, 122,* 202–211. DOI 10.1016/j.carbpol.2014.12.081.

45. Bendahou, A., Hajlane, A., Dufresne, A., Boufi, S., Kaddami, H. (2014). Esterification and amidation for grafting long aliphatic chains on to cellulose nanocrystals: a comparative study. *Research on Chemical Intermediates, 41(7),* 4293–4310. DOI 10.1007/s11164-014-1530-z.

46. Bendahou, A., Habibi, Y., Kaddami, H., Dufresne, A. (2009). Physico-chemical characterization of palm from Phoenix Dactylifera-L, preparation of cellulose whiskers and natural rubber–based nanocomposites. *Journal of Biobased Materials and Bioenergy, 3(1),* 81–90. DOI 10.1166/jbmb.2009.1011.

47. Jia, Z., Luo, Y., Guo, B., Yang, B., Du, M. et al. (2009). Reinforcing and flame-retardant effects of halloysite nanotubes on LLDPE. *Polymer-Plastics Technology and Engineering, 48(6),* 607–613. DOI 10.1080/03602550902824440.

48. Kapur, G. S., Brar, A. S. (1991). 13C-NMR studies of compositional and configurational sequence distribution in acrylonitrile–ethyl methacrylate copolymers. *Journal of Polymer Science Part A: Polymer Chemistry, 29(4),* 479–487. DOI 10.1002/pola.1991.080290404.

49. Kadi, S., Djadoun, S., Sbirrazzuoli, N. (2013). Thermal behavior of poly (ethyl methacrylate-co-acrylonitrile) nanocomposites prepared in the presence of an Algerian bentonite via solution intercalation and in situ polymerization. *Journal of Thermal Analysis and Calorimetry., 119(2),* 1113–1122. DOI 10.1007/s10973-014-4263-8.

50. Kim, Y., Song, Y., Kim, H. (2018). Preparation of transparent cellulose film with controlled haze using halloysite nanotubes. *Cellulose, 25(2),* 1239–1248. DOI 10.1007/s10570-017-1625-y.

51. Yong, C., Mei, C., Guan, M., Wu, Q., Han, J. et al. (2018). A comparative study of different nanoclay-reinforced cellulose nanofibril biocomposites with enhanced thermal and mechanical properties. *Composite Interfaces, 25(4),* 301–315. DOI 10.1080/09276440.2018.1400271.

52. Penzel, E., Rieger, J., Schneider, H. A. (1997). The glass transition temperature of random copolymers: 1. Experimental data and the Gordon-Taylor equation*. *Polymer (Guildf), 38,* 325–337.

53. Schneider, H. A., Rieger, J., Penzel, E. (1997). The glass transition temperature of random copolymers: 2. Extension of the Gordon-Taylor equation for asymmetric Tg vs composition curves. *Polymer (Guildf), 38(6),* 1323–1337. DOI 10.1016/S0032-3861(96)00652-0.

54. Lin, N., Wei, S., Xia, T., Hu, F., Huang, J. et al. (2014). Green bionanocomposites from high-elasticity soft polyurethane and high-crystallinity rigid chitin nanocrystals with controlled surface acetylation. *RSC Advances, 4(90),* 49098–49107. DOI 10.1039/C4RA07899C.

55. Cao, X., Habibi, Y., Lucia, L. A. (2009). One-pot polymerization, surface grafting, and processing of waterborne polyurethane-cellulose nanocrystal nanocomposites. *Journal of Materials Chemistry, 19(38),* 7137–7145. DOI 10.1039/b910517d.

56. Wang, D., Yu, J., Zhang, J., He, J., Zhang, J. (2013). Transparent bionanocomposites with improved properties from poly(propylene carbonate) (PPC) and cellulose nanowhiskers (CNWs). *Composites Science and Technology, 85,* 83–89. DOI 10.1016/j.compscitech.2013.06.004.

57. Ten, E., Bahr, D. F., Li, B., Jiang, L., Wolcott, M. P. (2012). Effects of cellulose nanowhiskers on mechanical, dielectric, and rheological properties of poly(3-hydroxybutyrate-co-3-hydroxyvalerate)/cellulose nanowhisker composites. *Industrial & Engineering Chemistry Research, 51(7),* 2941–2951. DOI 10.1021/ie2023367.

58. Jiang, F., Esker, A. R., Roman, M. (2010). Acid-catalyzed and solvolytic desulfation of H_2SO_4-hydrolyzed cellulose nanocrystals. *Langmuir, 26(23),* 17919–17925. DOI 10.1021/la1028405.

59. Lin, N., Dufresne, A. (2014). Surface chemistry, morphological analysis and properties of cellulose nanocrystals with gradiented sulfation degrees. *Nanoscale, 6(10),* 5384–5393. DOI 10.1039/C3NR06761K.

60. Fortunati, E., Puglia, D., Luzi, F., Santulli, C., Kenny, J. M. et al. (2013). Binary PVA bio-nanocomposites containing cellulose nanocrystals extracted from different natural sources: Part I. *Carbohydrate Polymers, 97(2),* 825–836. DOI 10.1016/j.carbpol.2013.03.075.

61. López-Suevos, F., Eyholzer, C., Bordeanu, N., Richter, K. (2010). DMA analysis and wood bonding of PVAc latex reinforced with cellulose nanofibrils. *Cellulose, 17(2),* 387–398. DOI 10.1007/s10570-010-9396-8.

62. Hamou, K. B., Kaddami, H., Dufresne, A., Boufi, S., Magnin, A. et al. (2018). Impact of TEMPO-oxidization strength on the properties of cellulose nanofibril reinforced polyvinyl acetate nanocomposites. *Carbohydrate Polymers, 181,* 1061–1070. DOI 10.1016/j.carbpol.2017.11.043.

63. Prashantha, K., Lecouvet, B., Sclavons, M., Lacrampe, M. F., Krawczak, P. (2012). Poly(lactic acid)/halloysite nanotubes nanocomposites: structure, thermal, and mechanical properties as a function of halloysite treatment. *Journal of Applied Polymer Science, 128,* 1895–1903.

64. Alloin, F., Aprea, A. D., El, N., Dufresne, A., Bossard, F. (2010). Nanocomposite polymer electrolyte based on whisker or microfibrils polyoxyethylene nanocomposites. *Electrochimica Acta, 55(18),* 5186–5194. DOI 10.1016/j.electacta.2010.04.034.

65. Alhuthali, A., Low, I. M. (2013). Water absorption, mechanical, and thermal properties of halloysite nanotube reinforced vinyl-ester nanocomposites. *Journal of Materials Science, 5(12),* 4260–4273. DOI 10.1007/s10853-013-7240-x.

66. Alamri, H., Low, I. M. (2012). Microstructural, mechanical, and thermal characteristics of recycled cellulose fiber-halloysite-epoxy hybrid nanocomposites. *Polymer Composites, 33(4),* 589–600. DOI 10.1002/pc.22163.

67. Low, I. M., Somers, J., Kho, H. S., Davies, I. J., Latella, B. A. (2009). Fabrication and properties of recycled cellulose fibre-reinforced epoxy composites. *Composite Interfaces, 16(7-9),* 659–669. DOI 10.1163/092764409X12477417562210.